Journal of Power Sources 202 (2012) 70–77

Contents lists available at SciVerse ScienceDirect

Journal of Power Sources

journal homepage: www.elsevier.com/locate/jpowsour

Novel nanostructured high-performance anion exchange ionomers for anion exchange membrane fuel cells

Lu Sun [a], Junsong Guo [a], Jie Zhou [a], Qingming Xu [a], Deryn Chu [b], Rongrong Chen [a,*]

[a] Richard G. Lugar Center for Renewable Energy, Indiana University-Purdue University Indianapolis, IN 46202, USA
[b] Army Research Laboratory, Adelphi, MD 20783, USA

ARTICLE INFO

Article history:
Received 27 September 2011
Received in revised form 6 November 2011
Accepted 7 November 2011
Available online 17 November 2011

Keywords:
Ionomer
Block copolymers
Self-assembly
Quaternary ammonium
Anion-exchange-membrane fuel cells

ABSTRACT

A novel block copolymer, styrene–ethylene/butylene–styrene (SEBS), was chosen as the starting material to prepare pendant quaternary ammonium-based ionomers with an ion-exchange-capacity (IEC) of 0.66, 1.30, and 1.54 mequiv. g^{-1}, denoted by QSEBS-L, QSEBS-M, and QSEBS-H, respectively. These QSEBS ionomers have been demonstrated to have excellent dimensional stability against hydration without significantly sacrificing the ionic conductivity as compared to the widely studied polysulfone (PSf)-based ionomers. The water uptake of the QSEBS-based ionomers depended on their functionality; a higher IEC in the ionomer resulted in more water uptake and a higher ionic conductivity. The MEAs fabricated with the QSEBS-M and QSEBS-H ionomers showed the best H_2/O_2 fuel cell performance with peak power densities reaching 210 mW cm^{-2} at 50 °C, which was significantly higher than that of the PSf-based ionomers (~30 mW cm^{-2}). Electrochemical impedance spectroscopy (EIS) analysis indicated that the superior fuel cell performance observed with the QSEBS-based ionomers can be attributed to: (1) the low internal cell resistance, and (2) the low charge transfer resistance in both the anode and the cathode due to the excellent dimensional stability and the balanced conductivity-hydrophobicity originated by the unique morphology of the QSEBS-based ionomers. AFM phase imaging measurements of the QSEBS-based ionomers revealed unique nanostructures containing isolated hydrophobic and continuous anion conducting hydrophilic domains. By further optimizing the chemistry and morphology of the ionomers and the membranes, the resistance of the anode and cathode of the AEMFCs will be further reduced. The performance of anion-exchange-membrane fuel cells will be further improved.

1. Introduction

With recent oil shortages and soaring energy prices, research for cleaner alternative energy sources has become a top priority in many nations. Fuel cell technology has been recognized as a clean and efficient energy source for a wide range of applications. Over the past few decades, significant research and development efforts have been focused on proton exchange membrane fuel cells (PEMFCs) due to their high energy density and well-established perfluoro-membrane and ionomer [1–4]. However, state-of-the-art PEMFCs are still facing challenges for commercialization due to high material and manufacturing costs, especially with the recently soaring platinum prices (~$1800 oz^{-1}). In recent years, there has been a growing interest in developing anion exchange membrane fuel cells (AEMFCs) as a potentially low-cost alternative to PEMFCs. Compared to PEMFCs, AEMFCs possess several important advantages, including (1) facile kinetics at the cathode, (2) a wide choice of fuels such as hydrogen, methanol, ethanol, or hydrazine, and (3) low materials and manufacturing costs [5–8]. However, only modest AEMFC performance has been reported so far, mainly due to the lack of satisfactory anion conducting ionomer catalyst binders and membranes available to the scientific community [9,10]. Furthermore, research papers dedicated to ionomer binder developments are rare.

In 2006, Varcoe et al. [11,12] reported a technology breakthrough in making membrane electrode assemblies (MEAs) for AEMFCs by depositing polyvinyl benzyl chloride (PVBC) on the electrodes followed by cross-linking and quaternizing the PVBC with aliphatic tertiary diamine to render the conductivity and insolubility of the ionomer binder in water. MEAs containing this PVBC polymer interface showed a substantial increase in the peak power density in a H_2/O_2 AEMFC at 50 °C (from 1.6 to 55 mW cm^{-2}). A polysulfone (PSf) pendant quaternary ammonium ionomer in MEA preparations was reported by Park [13] and Zhuang [14,15], respectively. Approaches using partially cross-linked and low functionality PSfs were adapted in preparing the PSf ionomers to ensure the ionomers remained intact in an aqueous solution. The best reported H_2/O_2 fuel cells with MEAs containing PSf ionomers had

* Corresponding author. Tel.: +1 317 274 4280; fax: +1 317 278 0789.
E-mail address: rochen@iupui.edu (R. Chen).

0378-7753/$ – see front matter © 2011 Elsevier B.V. All rights reserved.
doi:10.1016/j.jpowsour.2011.11.023

a peak power density of about 120 mW cm^{-2} at 60 °C [14]. Yan et al. [9] claimed that a quaternary phosphonium pendent PSf ionomer, soluble in low-boiling-point solvents, exhibited exceptional anion conductivity and better alkaline stability. A peak power output of 138 mW cm^{-2} in a H_2/O_2 AEMFC was achieved at 50 °C with 35 psi back pressure, 3.5 times higher than that of an MEA without ionomers. The significantly improved power capacity was attributed solely to the strong basicity of the quaternary phosphonium pendent PSf ionomer.

The chemistry–morphology–performance relationship of ionomer binders in AEMFCs has not been explored until a recent attempt by Atanassov et al. [16]. Widely reported PSf-based ionomers were compared with a novel poly(phenylene)-based ionomer in KOH free H_2/O_2 (or air) fuel cells. Variations in AEMFC performance were correlated to the reactant transportation influenced by the void volume in the electrode, and the catalyst–ionomer–gas interface was affected by hydration. The fuel cell performance of several other ionomers [17,18] from the industry has been briefly reported, but neither the formulation of the ionomers nor their functioning mechanisms were disclosed.

This research work aims to achieve a fundamental understanding of how the chemistry, morphology, and properties of ionomer binders affect the performance of AEMFCs. Desired characteristics of ionomer binders for preparing electrodes include (1) being soluble in a solvent of catalyst ink but insoluble in water, methanol, or ethanol; (2) having good mass transport for OH^-, H_2O, O_2, or H_2; (3) having good thermal/chemical stability; (4) having no poisoning effect on the catalysts; (5) having minimal swelling from hydration; (6) forming the optimal interfaces with catalysts and membranes. Nanostructured block copolymer-based SEBS ionomers with three functionalities as catalyst binders vs. the popular PSf-based ionomer were designed and synthesized. The ion conductivity, water uptake, and degree of swelling in the 100% hydrated state of these ionomers as a function of ion exchange capacity (IEC) were characterized. The morphology of various ionomers was studied by atomic force microscopy (AFM) in a phase imaging mode. The performance of the membrane electrode assemblies (MEAs) prepared with catalyst inks containing various ionomer binders and the same type of commercial membranes was tested in H_2/O_2 AEMFCs. Electrochemical impedance spectroscopy (EIS) was used to characterize how the physical and chemical characteristics of the ionomer binders affect the performance of the MEAs.

2. Experimental

2.1. Ionomer synthesis

Kraton G SEBS A1535 H and Polysulfone (Sigma Aldrich) were purified by precipitation from a 5 wt.% chloroform solution to methanol before chloromethylation. Chloromethylation was carried out following a modified procedure disclosed in our previous work [19]. Specifically for the chloromethylated SEBS (CMSEBS), 2.5 ml of chloromethyl methyl ether was diluted in 10 ml of chloroform followed by the slow addition of 30 μl of $SnCl_4$ in a three-neck flask equipped with a condenser in an oil bath at 65 °C. After mixing for 30 min, a 5 wt.% SEBS (2 g) chloroform solution was added to the above mixture drop-wise. The solution was stirred for 6–48 h at 65 °C (chloromethyl functionality was controlled by conversion, which was monitored by ^{1}H NMR recorded on a 500 MHz NMR (Bruker Avance II 500 MHz) spectrometer in $CDCl_3$, as shown in Fig. 1). The crude CMSEBS was precipitated in a methanol solution, and then washed several times with methanol before being vacuum dried overnight at room temperature. Quarternized SEBS (QSEBS) ionomers were derived from the amination of the CMSEBS with trimethylamine. First, 2 g of CMSEBS was dissolved in 40 ml of THF. Then, 10 ml of methanol was added to the solution to ensure no gelation or precipitation occurred during the quaternization reaction. 2 mole folds of trimethylamine, relative to the chloromethyl group, were slowly added to the solution with adequate agitation. The solution was kept at 40 °C for at least 12 h to guarantee a complete conversion.

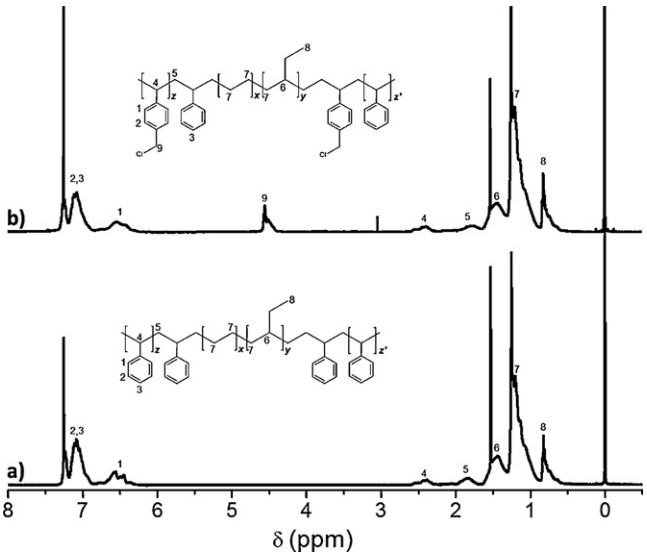

Fig. 1. ^{1}H NMR spectra of (a) Kraton G SEBS A1535 H and (b) CMSEBS-M in chloroform-d.

2.2. NMR characterization

A ^{1}H NMR (500 MHz) analysis of SEBS for both the starting material and the CMSEBS was performed on a Bruker Avance II 500 MHz instrument using chloroform-d as the solvent and tetramethylsilane (TMS) as the internal reference. Since the final ionomers after amination were insoluble in chloroform-d, NMR spectra were not acquired.

2.3. Ionic conductivity

QSEBS and QPSf ionomers were cast into thin membranes (~15 μm thick) by slowly evaporating the solvents on a PTFE substrate. Membranes were immersed in 1 M KOH for 48 h to exchange the Cl^- with OH^-. The OH^- ionic conductivity of the ionomer was measured using AC impedance spectroscopy with a Solartron 1250 frequency response analyzer interfaced with a Solartron 1287 potentiostat/galvanostat. The measurements were conducted in a galvanostatic mode with set frequencies ranging from 0.1 Hz to 60 kHz with the galvanostatically controlled AC current as 5 mA. A standard four-probe conductivity cell (BekkTech LLC, Loveland, CO) was used to assemble membrane test samples. The area resistance of the membrane was determined in de-ionized water at 30 °C, 40 °C, 50 °C, 60 °C, and 80 °C, respectively. Ionic conductivity was calculated as follows:

$$\sigma = \frac{L}{RTW} \quad (1)$$

where L is the length of the membrane between two potential sensing platinum wires in centimeters (cm), R is the membrane resistance in ohms (Ω), T is the thickness of the membrane in cm and W is the width of the membrane in cm.

Table 1
Basic properties of Tokuyama A901 membrane [17].

Thickness (μm)	ICE (mmol g^{-1})	Water content	OH^- conductivity (mS cm^{-2})	Burst strength (MPa)	Dimensional change wet ⇔ dry
10	1.7	0.15	29	0.2	MD/1% TD/4%

2.4. Ion-exchange capacity (IEC)

The IEC of the ionomer was determined by the back titration method. Around 200 mg of ionomer membranes (in OH^- form) were immersed in 20 ml of a 0.1 M HCl standard solution for 48 h. The solution was then titrated with a standard solution of potassium hydroxide (0.1 M) to pH 7. After titration, the membrane was soaked in 0.1 M HCl for 48 h then washed and immersed in DI water for 48 h to remove the remaining HCl. It was then vacuum dried at 70 °C for 24 h before being weighed to determine the dry mass (in Cl^- form). The IEC of the membrane was calculated by

$$\text{IEC} \quad (\text{mequiv./g}) = \frac{M_i - M_f}{m_d} \tag{2}$$

where M_i is the milliequivalents (mequiv.) of HCl before membrane neutralization, M_f is the mequiv. of HCl measured after neutralization, and m_d is the mass of the dried membrane in grams with Cl^- form.

2.5. Water uptake

The weight differences of membranes before and after soaking in DI water at room temperature for 24 h were used to calculate the water sorption of the membranes. The membranes were weighed immediately after being removed from DI water and after gently blotting the excess water from the surface with tissue paper. Then the membranes were dried overnight at 70 °C by vacuum. The dry membranes were transferred immediately to a dessicator before being cooled to room temperature. The dry membrane weights were recorded and the water sorption of the membranes were calculated by

$$\text{Water} \quad \text{sorption} \quad (\%) = \frac{W_{wet} - W_{dry}}{W_{dry}} \times 100 \tag{3}$$

where W_{wet} is the weight of wet membranes in OH^- forms in grams, and W_{dry} is the weight of dry membranes in OH^- forms in grams.

2.6. Swelling

In order to compare our results with data reported in the literature, we adopted the same test procedures described by Pan [14]. The cast thin ionomer membranes in Cl^- form were soaked in a 1 M KOH solution for 24 h. The dimension of the wet membranes was measured after quickly wiping the excess water from the surface. Swelling was measured in a lengthwide direction by recording the dimensions of the dry membranes and the wet membranes and was calculated using the following equation

$$\text{Swelling} \quad (\%) = \frac{L_{wet} - L_{dry}}{L_{dry}} \times 100 \tag{4}$$

where L_{wet} is the length of wet membranes in cm, and L_{dry} is the length of dry membranes in cm.

2.7. Atomic force microscopy (AFM)

QSEBS and QPSf ionomer THF/methanol solutions in Cl^- forms were diluted to around 0.5 wt.%. The solutions were sprayed onto a mica substrate to form a thin film (around 20 mg cm^{-2}) after the solvent evaporated. Films were vacuum dried at room temperature overnight before being imaged with the AFM. Films were also hydrated in a 0.1 M KOH solution for 12 h before the AFM experiment to compare the morphological changes in the hydrated state vs. the dry state.

The AFM experiments were carried out with an Agilent Technologies 5500 scanning probe microscope (SPM) in Acoustic Alternating Current (AAC) Mode at room temperature. Point probe pulse/non-contact/long cantilever (PPP-NCL) tips were used in the experiments. The set-point used for imaging varied between 0.5 and 1.0 V. All AFM phase images are shown as recorded without any additional image processing.

2.8. MEA fabrication

Since the Tokuyama A901 membrane as a commercial product has been well characterized and has consistent physical and chemical properties, it was chosen as the membrane for making the MEAs in this work. The reported key properties of the Tokuyama A901 membrane are listed in Table 1 [17]. The prepared QSEBS and QPSf ionomers were used as the ionomer binders in preparing catalyst inks for the anodes and cathodes. The catalyst inks for both the anode and cathode consisted of 16 mg of carbon-supported Pt/C (50 wt.% Pt from Alfa Aesar), 2 ml of a THF/methanol mixed solvent, and the ionomer in a 90:10 as catalyst:ionomer weight ratio. After homogenizing by sonication, the ink was simply airbrushed onto a 6.25 cm^2 Tokuyama A901 membrane. The MEA was sandwiched between two pieces of Toray Carbon Paper TGP-H-090 to form a single cell with an active electrode area of 4.5 cm^2. A fuel cell test system (Scribner Associates Model 850e) was used for controlling the cell temperature, humidity, H_2 and O_2 flow rate, and backpressures. The temperature of the fuel cell was maintained with a tolerance of ±0.2 °C. Fuel cell performance and impedance were tested using an 8-channel Solartron 1470 cell tester. The fuel cells were operated at 50 °C and 20 psi backpressure for both H_2 and O_2 gases. Impedance spectra were recorded by superimposing a 10 mV ac signal on the cell voltage of 0.800 V in the potentiostatic mode with frequencies ranging from 100 K to 0.1 Hz. The electrochemical impedance spectra were simulated by ZSimpWin software.

3. Results and discussion

3.1. Design and synthesis of ionomers with various functionalities and chemistry

Sulfonated block and grafted copolymers with well-defined nanoscale morphology have shown combinations of high ion exchange capacity (IEC) and high mechanical strength properties, which are normally unachievable with homopolymer or statistical copolymer systems in a PEM [20,21]. Liu et al. [22] prepared AEMs from triblock styrene–ethylene/butylene–styrene (SEBS) with styrene/ethylene-butylene (w w^{-1}) = 29/71. However, problems arose due to the low styrene content: (1) The freedom to adjust the functionality was constrained by the low styrene composition (IEC = 0.3 mmequiv. g^{-1}); (2) According to our experiments, the derived chloromethylated SEBS (CMSEBS) underwent gelation or precipitation from the solution during amination, which makes the ionomer unsuitable to be used as a binder for preparing MEAs.

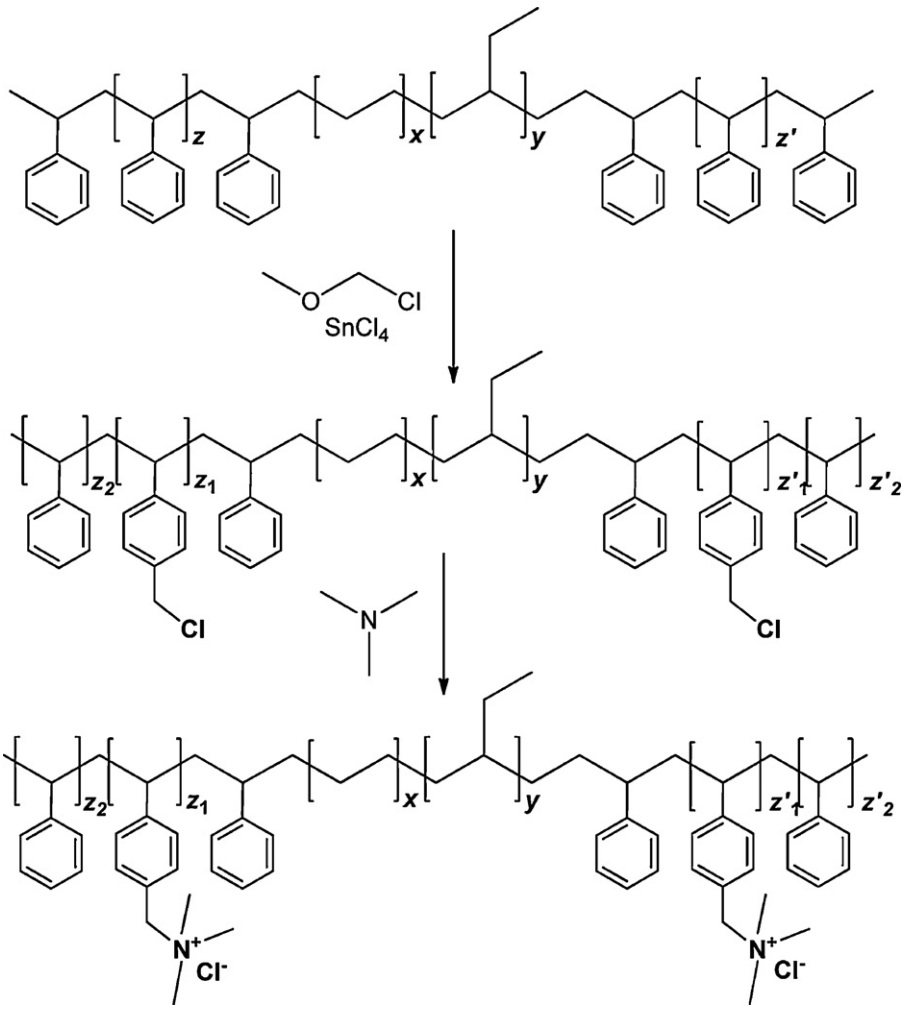

Scheme 1. The synthetic procedure of quaternary ammonium styrene–ethylene/butylene–styrene block copolymer ionomers (QSEBS) in Cl^- form.

We deliberately chose a commerically available SEBS with a styrene composition of 57 wt.% as the starting material to prepare ionomers with three IEC: 0.66, 1.30, and 1.54 mequiv. g^{-1} denoted by QSEBS-L, QSEBS-M, and QSEBS-H, respectively. As shown in Scheme 1, the chloromethylation reaction of the activated aryl ring on the SEBS block co-polymers (BCPs) took place in a diluted chloroform solution by chloromethyl methyl ether with a Tin(IV) catalyst at a reaction temperature of 65 °C. Compared to the chloromethylation of PSf, as discussed in our previous paper [19], the chloromethylation of the SEBS underwent gelation under the same reaction conditions. A more diluted solution and a relatively mild reaction temperature were used to prevent gelation. The highest IEC that can be achieved in a QSEBS ionomer is 1.58 mequiv. g^{-1}. The derived chloromethylated SEBS samples were further quarternized in a tetrahydrofuran (THF)/methanol solution by trimethylamine to prepare the QSEBS ionomer solutions. For comparison purposes, a PSf ionomer (QPSf) with an IEC of 1.28 mequiv. g^{-1} was also prepared following a modification of the procedure reported in our earlier work [14,19]. The prepared ionomer solutions in the Cl^- form were used as the binders to fabricate the MEAs.

^{1}H NMR was applied to characterize the chemical structures of the SEBS starting polymer and the chloromethylated SEBS, and the results (Fig. 1) indicate that the molecular structures changed during the chloromethylation process. Chloromethylation occurred at the activated aryl ring on the polystyrene blocks. The concentration of attached chloromethyl groups can be estimated from the integrated intensity of peak 9 (^{1}H NMR (500 MHz, chloroform-d, 25 °C, TMS): δ = 4.5 (s, 2H, CH_2)), in Fig. 1(b), to control the final ionomers with IEC levels of 0.66, 1.30, and 1.54 mequiv. g^{-1}, which were also validated by IEC testing (described in Section 2.4).

3.2. Physical properties of the prepared ionomers

Fig. 2 shows the ionic conductivity, the water uptake, and the dimensional stability (swelling) of the ionomers as a function of their IECs. The results are also summarized in Table 2. An IEC represents the ionomer functionality in unit weight, which is determined by the titration of the OH^- concentration in an ionomer using the procedure described in Section 2.4. Since the ionomers were designed to be used as the binders in preparing the MEAs, they were cast as very thin films with a thickness around 15 μm for physical property characterizations. If all the benzene rings in the SEBS were functionalized with OH^- groups, the theoretical maximum IEC in the SEBS would be ~4.2 mequiv. g^{-1}, which is much higher than the theoretical maximum IEC of 3.0 mequiv. g^{-1} for the PSf. However, due to the gelation that occurred during chloromethylation of the SEBS, the highest IEC that we could obtained was only 1.54 mequiv. g^{-1}, which is much lower than the 2.5 mequiv. g^{-1} that has been easily achieved in preparing PSf-based ionomers.

Our ionic conductivity, water uptake, and swelling test results of the baseline QPSf membranes with an IEC of 1.28 mequiv. g^{-1} agree well with those reported by Pan et al. [14]. A higher IEC in a SEBS-based ionomer led to a higher ionic conductivity. When the IEC

Table 2
IEC, anion conductivity, water uptake, and swell properties of QSEBS and QPSf ionomers at room temperature.

Sample	IEC [mequiv. g^{-1}]	Conductivity [mS cm^{-1}]	Water uptake [wt.%]	Swell ratio [%]
QPSf	1.28	12.0	237.8	52.0
QSEBS-L	0.66	3.0	48.8	1.8
QSEBS-M	1.30	7.8	184.7	12.3
QSEBS-H	1.54	9.6	265.2	18.7

increased from 0.66 to 1.54 mequiv. g^{-1}, the QSEBS ionic conductivity increased from 3.0 to 9.6 mS cm^{-1}. However, compared with QPSf ionomers [14,19], the QSEBS showed lower ionic conductivity, which indicated that ethylene/butylene hydrophobic components in the QSEBS reduced the ionic conductivity of the QSEBS. The QPSf ionomer with an IEC of 1.28 mequiv. g^{-1} had an ionic conductivity of 12 mS cm^{-1}, which is 54% higher than that of the QSEBS-M with a similar IEC. In addition, the water uptake of the three QSEBS-based ionomers showed a linear increase from 48.8 to 265.2 wt.% as the IEC increased. Again the hydrophobic nature of the polymer backbone expelled more water than the PSf, and at a similar IEC, the QPSf retained 22% more water than the QSEBS-M.

Although the QSEBS-based ionomers showed rather low ionic conductivity and less water uptake as compared to the QPSf ionomers, the dimensional stability of the QSEBS ionomers is the key advantage. In general, the degree of membrane swelling depends on the IEC, the composition and morphology of the ion exchange groups, the degree of cross-linkage, the pH of the solution, and the temperature. The membrane swells more with increasing IEC, which is shown in Fig. 2 for three QSEBS. The QSEBS with the lower IEC showed less membrane swelling. Due to a tendency of wrinkling on the thin membrane surfaces, we measured the expansion of the membranes only in a lengthwide direction, as was also done by others [14]. All three QSEBS ionomers showed less than 20% swelling in the KOH solutions; however, the QPSf ionomer swelled to over 50%. The dimensional stability of the ionomer is very critical for achieving high performance MEAs, which will be demonstrated in the following fuel cell test section.

The ionic conductivities of the ionomers at elavated temperatures were characterized for the thermal stability of the block copolymer-based QSEBS ionomers vs. the PSf ionomer. As shown in Fig. 3, the ionic conductivities of the three QSEBS ionomers and the QPSf-based ionomer were characterized in DI water at a temperature range from 30 to 80 °C with a temperature control of ±0.1 °C. All the ionomers bearing quaternary ammonium functional groups revealed incremental ionic conductivity as the temperature increased without evidence of conductivity loss from degradation of the functional groups. All the ionomers were tested with complete removal of the KOH; the ionic conductivities were thus good indications of ionomer intrinsic basicity. Compared to the QSEBS ionomers, the QPSf ionomer had a much higher ionic conductivity over the whole range of testing temperatures, with the highest conductivity being 30 mS cm^{-1}. The ionic conductivities of the QSEBS ionomers also increased with temperature at a slightly lower gradient than that of the QPSf.

3.3. Nanostructured morphologies of the ionomers

AFM phase imaging was applied to characterize the morphology of the ionomers. The ionomer thin film specimens were prepared by the evaporation of the solvent from a diluted ionomer solution, a similar procedure to that of electrode fabrication, except no catalyst was added. QSEBS ionomers with covalently bonded dissimilar blocks, i.e. hydrophilic functional styrene blocks and hydrophobic ethylene/butylene blocks, tend to form clear phase separations. As shown in Fig. 4(a–c), well-defined phase segregations were observed on all three QSEBS ionomers. The dark isolated domains were assigned to the ethylene/butylene blocks [23], while the bright continuous phases represented the styrene blocks with pendent quaternary ammonium groups. By attaching more pendent functional groups in the QSEBS, the volume percentages of the styrene block increased, leading to an area increase in the continuous domains, and a decrease in the dark domains. To further study the structural stability of the ionomers in an alkaline solution, the thin ionomer films were immersed in a 0.1 M KOH solution for 24 h, then the AFM phase imaging was performed under a 100% hydrated condition. As shown in Fig. 4(a′–c′), the bright continuous domains swelled to different extents in all three QSEBS ionomer films after hydration. The ionomers with higher functionality showed more pronounced swelling. Nevertheless, the distinct phase separations

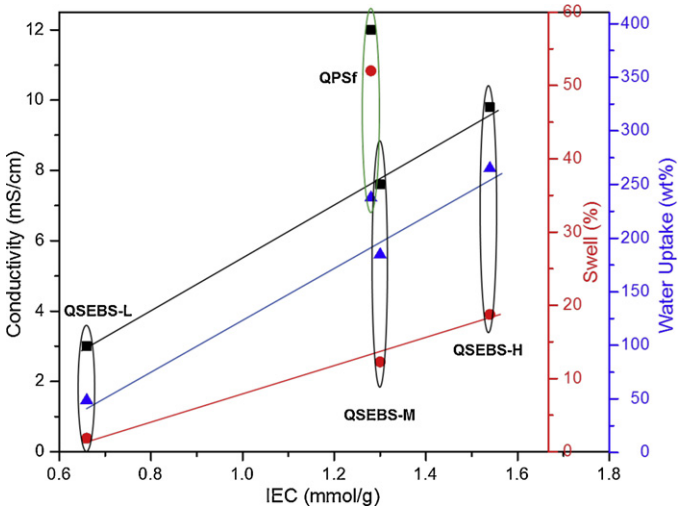

Fig. 2. Ionic conductivity (■), water uptake (▲), and swelling (●) properties as a function of IEC for QPSf and QSEBS ionomers at room temperature.

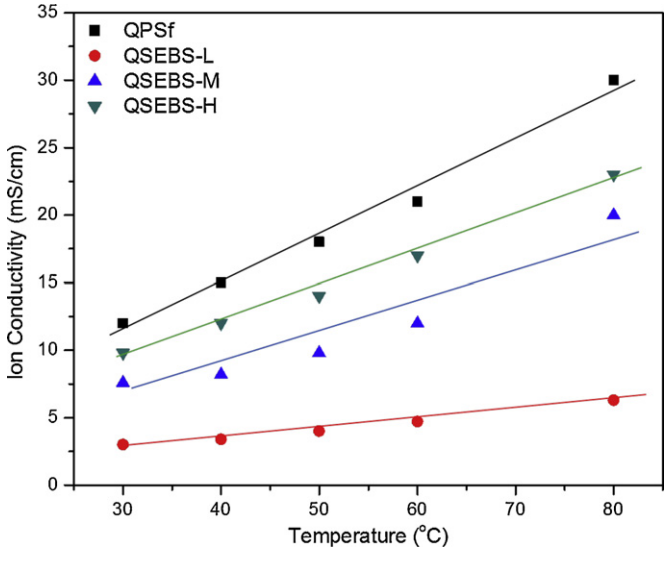

Fig. 3. Ionic conductivity of QPSf and QSEBS ionomers at different temperatures.

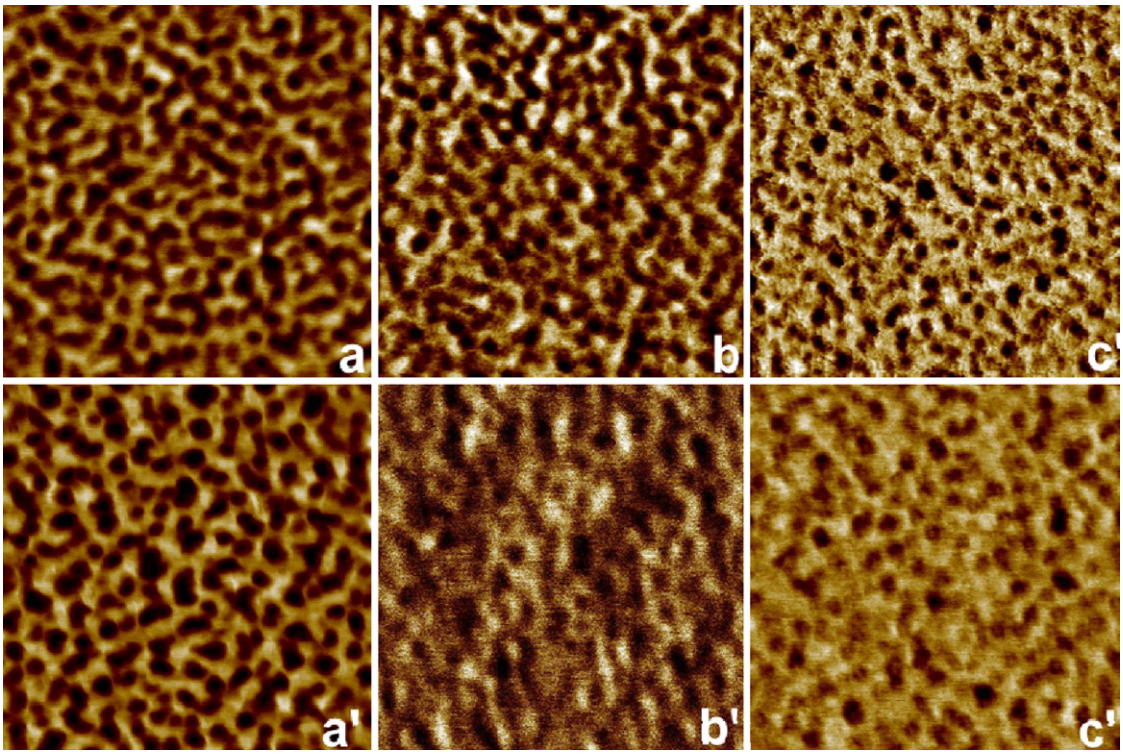

Fig. 4. AFM phase images (500 nm × 500 nm) of thin films from (a–a′) QSEBS-L, (b–b′) QSESB-M and (c–c′) QSEBS-H in dry (a–c) and hydrated states (a′–c′). See experimental Section 2.7 for the AFM measurement procedure.

were still preserved. The unique nanostructures of the QSEBS-based ionomers can be attributed to the lower water uptake and the good dimensional stability discussed above. The incorporated hydrophobic nano-domains tend to drive excess water away, thus reducing the QSEBS-based ionomer water uptake as compared to the PSf ionomer with a similar IEC.

3.4. H_2/O_2 fuel cell performance and electrochemical impedance spectroscopy

The polarization and power curves presented in Fig. 5 are the results of H_2/O_2 AEMFCs using Tokuyama A901 membranes.

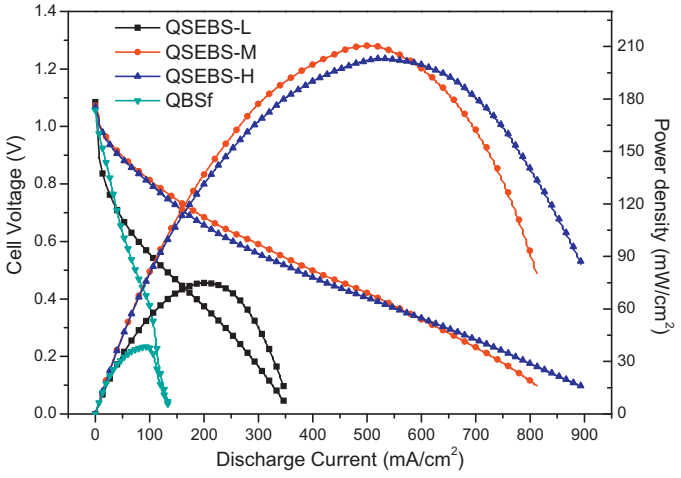

Fig. 5. *I–V* polarization and power density curves of MEAs fabricated with QPSf and QSEBS ionomer binders, and Tokuyama A901 membranes. Test conditions: Pt loading = 1.28 mg cm^{-2} for both the cathode and anode; cell and H_2/O_2 humidifier temperatures = 50 °C; H_2 and O_2 flow rates = 200 sccm at 20 psi back pressure, 100% RH.

All the test cells were assembled with the Tokuyama A901 membrane; only the ionomer binders used in the anodes and cathodes were different. Operating at 50 °C and 20 psi backpressure for H_2/O_2, the AEMFCs with QSEBS ionomers in both the anode and cathode outperformed that with the QPSf ionomer under the same test conditions. The QSEBS ionomers with an IEC higher than 1.30 mequiv. g^{-1} showed much better fuel cell performance than the QSEBS ionomers with low functionality (IEC ~ 0.66 mequiv. g^{-1}). The best cell performance was observed on the MEAs fabricated with QSEBS-H and QSEBS-M, which showed a peak power density over 210 mW cm^{-2} when the current density was 500–550 mA cm^{-2} and the cell voltage was 0.40 V. These results indicate that QSEBS ionomers with higher functionality tend to have lower ionic transport resistance and higher efficiency of the catalysts in the electrodes due to the larger number of ionic conducting sites, which are proven by electrochemical impedance spectroscopy (EIS) measurements, as discussed later. Interestingly, although the QPSf had a higher OH^- conductivity than all of the QSEBS ionomers (Fig. 3), the cell voltages dropped sharply with increased current density, and the power density was rather low. A peak power of less than 30 mW cm^{-2} was achieved on the electrode prepared with the QPSf, agreeing with Atanassov's report [7]. The poor fuel cell performance of the QPSf ionomer indicates that the OH^- conductivity in the catalyst layer played only a partial role; other properties, such as comparability of the ionomer with the membrane (Tokuyama A901), water uptake and swelling, are also critical factors to consider for achieving optimal catalyst–ionomer–gas interfaces, and satisfactory gas and water transports in the electrodes.

To further understand the effects of ionomers on AEMFC performance, EIS were recorded on the cells during the discharge test at 50 °C with cell voltage at 0.800 V. As shown in Fig. 6, both of the AEMFCs with either QEBS-H or QSEBS-M had similar EIS characteristics, while the AEMFCs with QSBS-L or QPSf had significantly enlarged EIS characteristics. With the assumption that the mass

Table 3
Summary of fitting parameters using the equivalent circuit (Fig. 7) for modeling the EIS.

	$R_{a,ct}$ (Ω cm^2)	CPE_a, Q (F cm^{-2})	CPE_a, n	R_i (Ω cm^2)	$R_{c,ct}$ (Ω cm^2)	CPE_c, Q (F cm^{-2})	CPE_c, n
QPSf	3.216	0.002484	0.6366	0.3352	2.989	0.02215	0.7222
QSEBS-L	2.837	0.0003262	0.7851	0.2267	3.988	0.00209	0.7402
QSEBS-M	0.7103	0.002104	0.8047	0.1455	0.8774	0.09174	0.7169
QSEBS-H	0.5682	0.00207	0.8201	0.1283	1.07	0.08738	0.7197

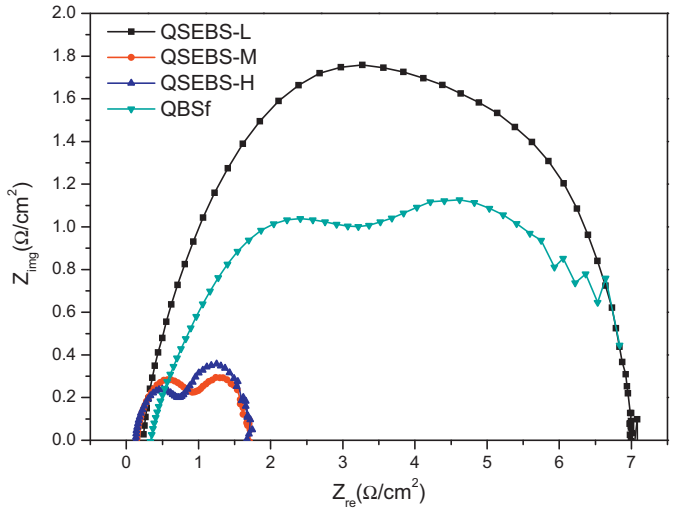

Fig. 6. Electrochemical impedance spectra of the fuel cells with different ionomers at a cell voltage of 0.80 V, 100% RH and 20 psi backpressure for H_2/O_2.

transport at the anode and cathode is not a limiting factor at 0.800 V, the measured impedance spectra can be modeled by the equivalent circuit, as shown in Fig. 7. The fitting parameters for the equivalent circuit are summarized in Table 3. Here, R_i is the fuel cell internal resistance and $R_{a,ct}$ and $R_{c,ct}$ are the charge transfer resistances at the anode and the cathode, respectively. The constant phase elements CPE_a and CPE_c were used in the simulation due to the nature of the porous electrodes. For all test AEMFCs, the same type of membrane (A901) was used. Therefore, the changes in R_i of these AEMFCs can be mainly attributed to the various ionomers in the electrodes. Agreeing with the ionic conductivity results presented in Fig. 3, the R_i of the AEMFCs with various QSBS ionomers dropped with increasing IEC functionality of the ionomers, but was unexpectedly low for the AEMFC with the QPSf ionomer. Although QSBS-M and QSBS-H ionomers showed lower ionic conductivity than the QPSf in Fig. 3, they seem to be more comparable with the A901 membrane and result in a lower internal impedance R_i in the AEMFCs. The differences in the R_i of the various AEMFCs are not as significant as the differences in other parameters, e.g. $R_{a,ct}$ and $R_{c,ct}$. The AEMFCs with the QSBS-H and QSBS-M ionomers show significantly lower $R_{a,ct}$ and $R_{c,ct}$ impedance than those obtained with the QSBS-L and QPSf ionomers, which could explain

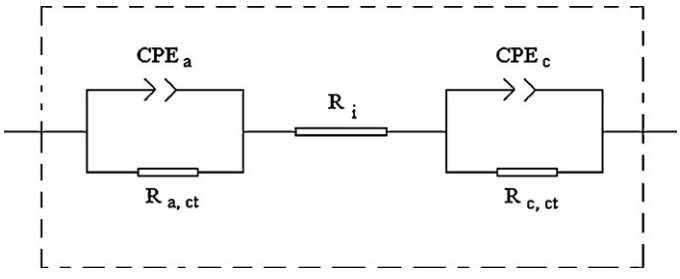

Fig. 7. Equivalent circuit for modeling the electrochemical impedance spectra of the fuel cells with different ionomers.

the superior fuel cell performance using the QSBS-M and QSBS-H ionomers. Optimal water uptake, better dimensional stability, and the unique morphology of the QSEBS ionomers with IEC higher than 1.30 mequiv. g^{-1} seem to provide the optimum charge transport, mass transport, and ionic transport in the electrodes. Compared to the QSEBS-L ionomer, the QSEBS ionomers with higher functionality were expected to have lower ionic transport resistance and higher efficiency of the catalysts in the electrodes due to the larger number of ionic conducting sites at both the anode and cathode. These results were confirmed by the low anode and cathode charge transfer resistance ($R_{a,ct}$ and $R_{c,ct}$) observed. Further reducing the $R_{a,ct}$ and $R_{c,ct}$ of the AEMFCs with improved ionomers and membranes will result in AEMFC performance that can be comparable to or better than state-of-the-art PEMFCs.

4. Conclusions

In this work, nanostructured triblock SEBS with pendant quaternary ammonium-based ionomers were synthesized by chloromethylation followed by amination. These SEBS ionomers demonstrated excellent dimensional stability against hydration without significantly sacrificing the ionic conductivity, as compared to the PSf-based ionomer. AFM imaging revealed that the improvement in the dimensional stability can be attributed to the unique nanostructures observed on the SEBS ionomers. The electrodes prepared with ionomers based on block copolymer SEBSs show 4–5 times higher power density than those with PSf-based ionomers in H_2/O_2 AEMFCs. The EIS analysis indicates a significant reduction in the resistance of charge transport in both the anode and cathode with the SEBS-based ionomers over the PSf-based ionomer with similar IECs. AFM phase imaging and electrochemical impedance spectroscopy have been demonstrated to be very useful techniques to study the structure and performance of ionomers in AEMFCs. By further optimizing the chemistry and morphology of the ionomers and the membranes, the resistance of the anode and cathode of the AEMFCs will be further reduced. With continued development, the performance and power capacity of AEMFCs will be comparable to or better than that of state-of-the-art PEMFCs.

Acknowledgements

This work was sponsored by the Army Research Laboratory (Grant no. W911NF-10-2-0075). The Kraton G SEBS A1535 H sample was kindly provided by Kraton Performance Polymers, Inc.

References

[1] J. Weber, K.D. Kreuer, J. Maier, A. Thomas, Adv. Mater. 20 (2008) 2595.
[2] M.P. Nieh, M.D. Guiver, D.S. Kim, J.F. Ding, T. Norsten, Macromolecules 41 (2008) 6176.
[3] M.S. Whittingham, R.F. Savinelli, T.A. Zawodzinski, Chem. Rev. 104 (2004) 4243.
[4] C.H. Lee, H.B. Park, Y.M. Lee, R.D. Lee, Ind. Eng. Chem. Res. 44 (2005) 7617.
[5] G.F. McLean, T. Niet, S. Prince-Richard, N. Djilali, Int. J. Hydrogen Energy 27 (2002) 507.
[6] J.R. Varcoe, R.C.T. Slade, Fuel Cells 5 (2005) 187.
[7] B.Y.S. Lin, D.W. Kirj, S.J. Thorpe, J. Power Sources 161 (2006) 474.
[8] P.K. Shen, C. Xu, H. Meng, R. Zeng, Adv. Fuel Cells (2005) 149.
[9] S. Gu, R. Cai, T. Luo, Z.W. Chen, M.W. Sun, Y. Liu, G.H. He, Y.S. Yan, Angew. Chem. Int. Ed. 48 (2009) 6499.

[10] T.J. Clark, N.J. Robertson, H.A. Kostalik, E.B. Lobkovsky, P.F. Mutolo, H.D. Abruna, G.W. Coates, J. Am. Chem. Soc. 131 (2009) 12888.
[11] J.R. Varcoe, R.C.T. Slade, Electrochem. Commun. 8 (2006) 839.
[12] J.R. Varcoe, R.C.T. Slade, E. Lam How Yee, Chem. Commun. (2006) 1428.
[13] J.S. Park, S.H. Park, S.D. Yim, Y.G. Yoon, W.Y. Lee, C.S. Kim, J. Power Sources 178 (2008) 620.
[14] J. Pan, S.F. Lu, Y. Li, A.B. Huang, L. Zhuang, J.T. Lu, Adv. Funct. Mater. 20 (2010) 312.
[15] S.F. Lu, J. Pan, A.B. Huang, L. Zhuang, J.T. Lu, Proc. Natl. Acad. Sci. U.S.A. 105 (2008) 20611.
[16] E.E. Switzer, T.S. Olson, A.K. Datye, P. Atanassov, M.R. Hibbs, Cy. Fujimoto, C.J. Cornelius, Electrochim. Acta 55 (2010) 3404.
[17] H. Yanagi, K. Fukuta, ECS Trans. 16 (2008) 257.
[18] M. Piana, M. Boccia, A. Filpi, E. Flammia, H.A. Miller, M. Orsini, F. Salusti, S. Santiccioli, F. Ciardelli, A. Pucci, J. Power Sources 195 (2010) 5875.
[19] G. Wang, Y. Weng, J. Zhao, D. Chu, D. Xie, R. Chen, Polym. Adv. Technol. 21 (2010) 554.
[20] Y.A. Elabd, M.A. Hickner, Macromolecules 44 (2011) 1.
[21] T.J. Peckham, S. Holdcroft, Adv. Mater. 22 (2010) 4667.
[22] Q.H. Zeng, Q.L. Liu, I. Broadwell, A.M. Zhu, Y. Xiong, X.P. Tu, J. Membr. Sci. 349 (2010) 237.
[23] R.S. Mclean, B.B. Sauer, Macromolecules 30 (1997) 8314.